Product Selectivity in Photochemical CO_2 Reduction by a Post-synthetically Modified Zr-MOF

Rosmi Reji,[1,4] Juan P. Vizuet,[1] Xiaoli Yan,[1,5] Biki K. Behera,[1] Xin Zheng,[1] Matthew Klenk,[2] Nicholas P. Weingartz,[3] George T. Kostopoulos,[1] Lin X. Chen,[3,4] Peter Zapol,[2] Neeraj Agarwal,[8] Eliu Huerta,[5,6] Murat Keceli,[7] and Ksenija D. Glusac*[1,4]

[1]Department of Chemistry, University of Illinois Chicago, Chicago, Illinois 60607, USA

[2]Materials Science Division, Argonne National Laboratory, Lemont, Illinois 60439, USA

[3]Department of Chemistry, Northwestern University, Evanston, Illinois 60201, USA

[4]Chemical Sciences and Engineering, Argonne National Laboratory, Lemont, Illinois 60439, USA

[5]Data Science and Learning Division, Argonne National Laboratory, Lemont, Ilinois 60439, USA

[6]Department of Computer Science, The University of Chicago, Chicago, Ilinois 60637, USA

[7]Computational Science Division, Argonne National Laboratory, Lemont, Illinois 60439, USA

[8]UM-DAE Centre for Excellence in Basic Sciences, University of Mumbai, Vidhyanagari Campus, Mumbai, 400098, India

ABSTRACT

Metal-organic frameworks (MOFs) are an excellent platform for photochemical CO_2 reduction into valuable chemicals. Herein, we report the synthesis and photocatalytic behavior of Ru@MOF-808, a Zr-based MOF that was post-synthetically modified with a Ru-polypyridyl complex. The post-synthetic modification was achieved using solvent-assisted incorporation of bipyridine-carboxylate ligands onto the nodes of the MOF-808, followed by the coordination of the Ru(II)-terpyridine moiety. A thorough characterization including ^{1}H-NMR, diffuse reflectance UV/Vis spectroscopy, X-ray absorption spectroscopy and gas adsorption studies, combined with DFT calculations, provides strong support for efficient incorporation of the molecular Ru-complex at the loading of one Ru center per node. In the presence of a strong sacrificial reductant BIH(1,3-Dimethyl-2-phenylbenzimidazoline), Ru@MOF-808 was found to catalyze photochemical reduction of CO_2 into a mixture of CO and formate ion. When compared to the homogeneous model catalyst $Ru(tpy)(bpy)_2^+$, Ru@MOF-808 was found to exhibit higher formate yields. To explain these formate enhancements, we propose a mechanism that involves CO_2 capture at the MOF nodes to form Zr-bicarbonate species, which further react in a hydride transfer reaction with photo-generated Ru-H donor, thereby outperforms molecular catalyst in $HCOO^-$ production. Overall, the results presented in this work indicate the potential of Zr-based MOFs in integrating CO2 capture with its photochemical conversion to desired products.

INTRODUCTION

Artificial photosynthesis, a process in which carbon dioxide is photochemically reduced to value-added products, represents an important approach toward carbon dioxide upcycling using renewable energy sources.[1–3] Metal-organic frameworks (MOFs),

modified with molecular catalysts and chromophores, are excellent "molecular photoreactors" for photochemical CO_2 reduction.[4] The molecular chromophores and catalysts are usually introduced into MOFs using post-synthetic methods that rely on the node functionalization with carboxylate-functionalized molecules,[5–7] metal coordination to bipyridine-based ligands,[8–10] or electrostatic interactions between the oppositely charged MOF and the molecular catalyst.[11,12] The immobilization of the catalysts into MOFs often increases their stability by preventing undesired decomposition pathways.[11,13,14] Furthermore, the MOF cavity provides three-dimensional scaffold for dynamic orientation of complex bimetallic catalytic motifs for target transformation.[6] The MOF scaffold also enables the integration of chromophores and catalysts in close proximity, greatly enhancing the photocatalytic performance relative to the homogeneous analogs.[10] The chemical tunability of molecular catalysts within the MOF enables efficient product selectivity enhancements. For example, Cu-based catalysts have been shown to selectively produce either carbon monoxide or formate ion, depending on the hydrogen-bonding stabilization effects provided by the ligand.[9] The MOFs with different pore sizes can affect photocatalytic performance via their different abilities to host chromophores and catalysts of different sizes.[15] While C1 products, such as CO, formate or methane, are usually formed, recent studies have shown that acetic acid can be formed using a Ce-based MOF.[8] Recent studies have also shown that integrated CO_2 capture and conversion can be achieved using ionic liquids.[16]

Ru-polypyridyl complexes with one or more labile ligands have been shown to catalyze electrochemical carbon dioxide reduction.[17] The reaction most often produces two-electron reduced products, carbon monoxide and formate.[5,16,18–24] The electron accumulation involves two ligand-centered reductions,[18] and the sequence of chemical and electron transfer steps can be controlled using steric effects.[20,21] The proposed mechanism for carbon monoxide formation involves the reaction of two-electron-reduced complex with CO_2 to form the metal-bound CO_2 adduct, which is further reduced, causing the loss of O^{2-} dianion and the formation of metal-bound carbon monoxide (M-CO).[18,23–25] The O^{2-} dianion is transferred either to protons to form water [23,24] or to CO_2 molecule to form the carbonate CO_3^{2-} dianion.[25,26] It was also found that O^{2-} transfer in the reductive disproportionation of CO_2 to CO and CO_3^{2-} was facilitated by flexible ligation of the methyl-substituted bipyridine ligand and the formation of a 5-membered metallacycle.[25] In the case of formate production, two different mechanisms have been proposed. One involves the reaction of OH- ions with M-CO intermediate to yield M-COOH adduct from which the formate ion is released.[23,24] A more commonly accepted mechanism involves the insertion of CO_2 into the Ru-H complex formed upon the protonation of the doubly reduced molecular precursor,[27] which is consistent with previous findings involving reactions of CO_2 with Ru-based hydrides.[28–31] The reduction that goes beyond the two-electron pathway, such as methanol has been demonstrated to occur from M-CO adduct at low temperatures using either electrochemical methods[32] or the utilization of recyclable organic hydrides.[33]

The photocatalytic carbon dioxide reduction by Ru-tpy based complexes have been hampered by their short-lived excited states.[34,35] While many Ru-based compounds exhibit long-lived triplet metal-to-ligand charge transfer (^{3}MLCT) states, the excited states of Ru-tpy complexes are short-lived (few hundred nanoseconds) due to the presence of close-lying triplet metal-centered (^{3}MC) states which tend to undergo rapid nonradiative decay to the ground state.[34] For this reason, Ru-tpy catalysts are often combined with light-harvesting chromophores to enable photocatalytic CO_2 reduction.[27] Despite their short-lived excited states, Ru-tpy complexes has been applied in direct photochemical reactions involving either photo-generation of a Ru-H complex[36] or photochemical reduction of CO_2.[37,38]

In this study, we report the synthesis of Ru@MOF-808, a MOF with benzene-1,3,5-tricarboxylate ligands and Zr-based nodes that are post-synthetically modified with Ru(tpy)(bpy)ACN^{2+} units (Scheme 1, tpy-terpyridine, bpy -5,5'-dimethyl-2,2'-bipyridine). Characterization revealed that the Ru-coordinated moieties in Ru@MOF-808 are structurally analogous to the molecular complex Ru(bpy)(tpy)$^{2+}$. Additionally, incorporating these moieties into MOF-808 at a loading of one Ru center per Zr node reduces the material's surface area by half. We investigated the photocatalytic CO_2 reduction activity of Ru@MOF-808 using different sacrificial electron donors and found that, in the presence of a strong reductant, conversion to C_1 products—CO and formate—occurs. Under photocatalytic conditions, Ru@MOF-808 generates more formate compared to the Ru(tpy)(bpy)ACN^{2+} model complex, which favors CO production. These results suggest that the MOF scaffold plays a key role in steering product distribution. Building on this study and our previous findings that CO_2 insertion into Zr nodes activates bound bicarbonates toward formate formation, we propose a mechanism involving photochemical reduction via hydride transfer between Zr-bound bicarbonate and a photogenerated Ru-hydride intermediate. This work highlights the ability of MOF-based nodes to enable cooperative catalysis by integrating substrate-binding sites with reduction-active moieties.

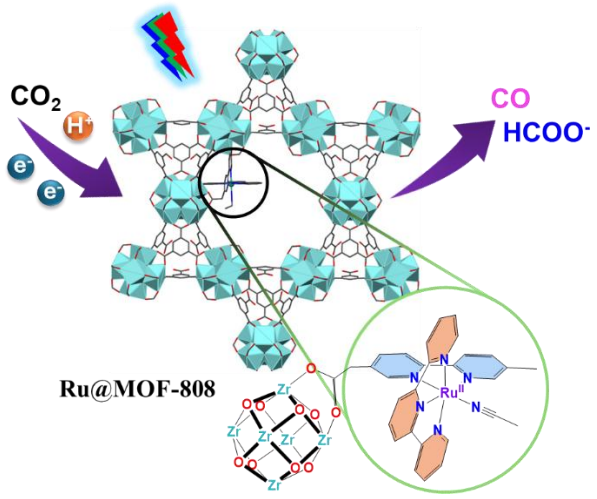

Scheme 1. Schematic illustration of photocatalytic CO_2 reduction into CO and $HCOO^-$ by Ru@MOF-808.

RESULTS AND DISCUSSION

Synthesis and characterization of Ru@MOF-808. MOF-808 was selected for this study due to the high stability of Zr-based MOFs.[39] Furthermore, the modulator molecules can be readily removed from the 6-connected Zr_6 node, resulting in open sites that can serve as anchoring points for a variety of molecules. The MOF-808 cavity (~16 Å) is constructed by the connection of tetrahedrons formed by four different Zr_6 nodes, and this cavity can be accessed through windows formed by six tetrahedrons (~10 Å). The synthesis of Ru@MOF-808 was achieved by a two-step process, as shown in Scheme 2. First, the carboxylated ligand bpy-COOH was grafted onto the modulator-free nodes of MOF-808 using solvent-assisted ligand incorporation.[7] Interestingly, the reaction between the resulting bpy@MOF-808 and $Ru^{III}(tpy)Cl_3$ did not yield the desired Ru@MOF-808 adduct. This lack of reactivity contrasts with the model compound, which readily forms the $Ru(II)(tpy)(bpy)^{2+}$ complex under similar conditions. We hypothesize that this difference in reactivity is due to the use of triethylamine (as a reducing agent for Ru^{III} to Ru^{II} conversion) which caused MOF degradation at elevated temperatures. To overcome this challenge, we synthesized Ru@MOF-808 using the $[Ru^{II}(tpy)(ACN)_3][PF_6]_2$ complex as a precursor (synthesis and characterization of precursors are described in supporting information, Section 1).

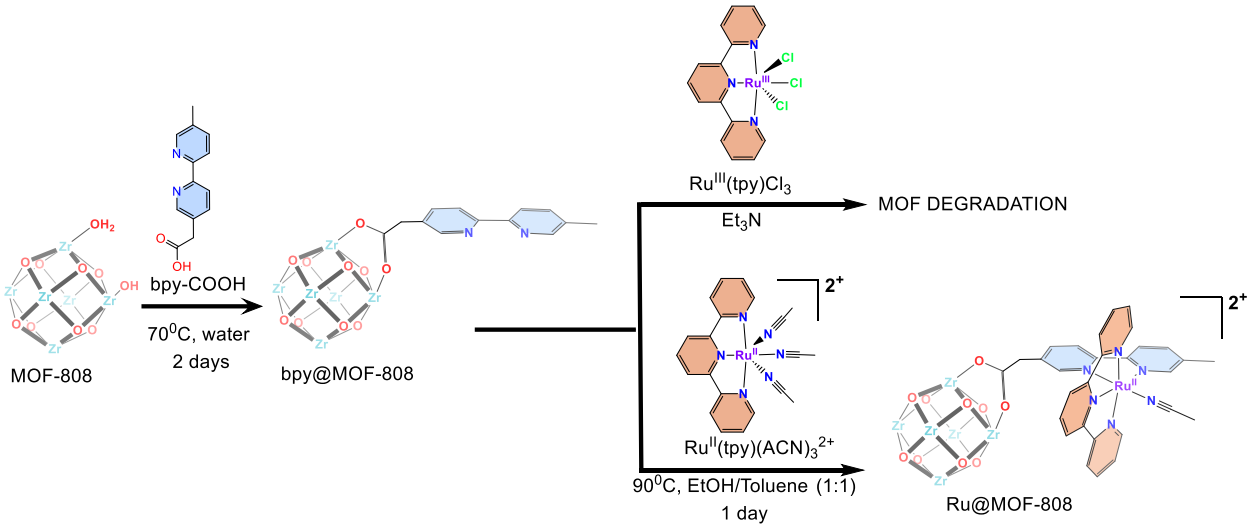

Scheme 2. Synthesis of Ru@MOF-808. The post-synthetic modification of MOF-808 with carboxylated bpy precursor afforded bpy@MOF-808. While the synthesis of Ru@MOF-808 did not proceed when Ru(III) precursor and triethyl amine were used, the reaction was successful when Ru(II) regent was employed.

The crystallinity of the samples remained unperturbed by the post-synthetic modifications, as confirmed using powder X-ray diffraction shown in Figure 1a. Different loadings of bpy ligands per node in MOF-808 were achieved by varying the concentration of bpy-COOH

(details in the supporting information). The ^{1}H NMR spectra of acid-digested bpy@MOF-808 samples with different bpy loadings are shown in Figure 1b. The MOF-808 ligand, benzene tricarboxylic acid, exhibits a single peak in the aromatic region at 8.66 ppm, which was used as a reference signal to evaluate the amount of bpy-COOH loading (integration was set to a value of 6, since there are two tricarboxylic acid ligands per Zr-node in MOF-808). The integration of NMR peaks associated with bpy-COOH in the 8.2-9 ppm range indicates that a loading of either approximately two or four bpy units per Zr-node was achieved. The quantification of Ru@MOF-808 was also achieved using ^{1}H NMR of digested samples. In this case, the samples were digested using basic conditions because the acid digestion generated paramagnetic Ru(III) species that made NMR measurements challenging. The ^{1}H NMR of the base-digested Ru@MOF-808 indicates that the bpy-COOH loading decreases after the reaction of bpy@MOF-808 with $Ru(tpy)(ACN)_3^{2+}$ to a value of less than one bpy ligand per node (Figure 1b). Thus, we conclude that Ru@MOF-808 contains less than one Ru-complex per node and this result is consistent with the elemental analysis (ICP-OES analysis indicates 0.8 Ru centers per node, suppoting Information, Section 1) and the gas adsorption experiments discussed below.

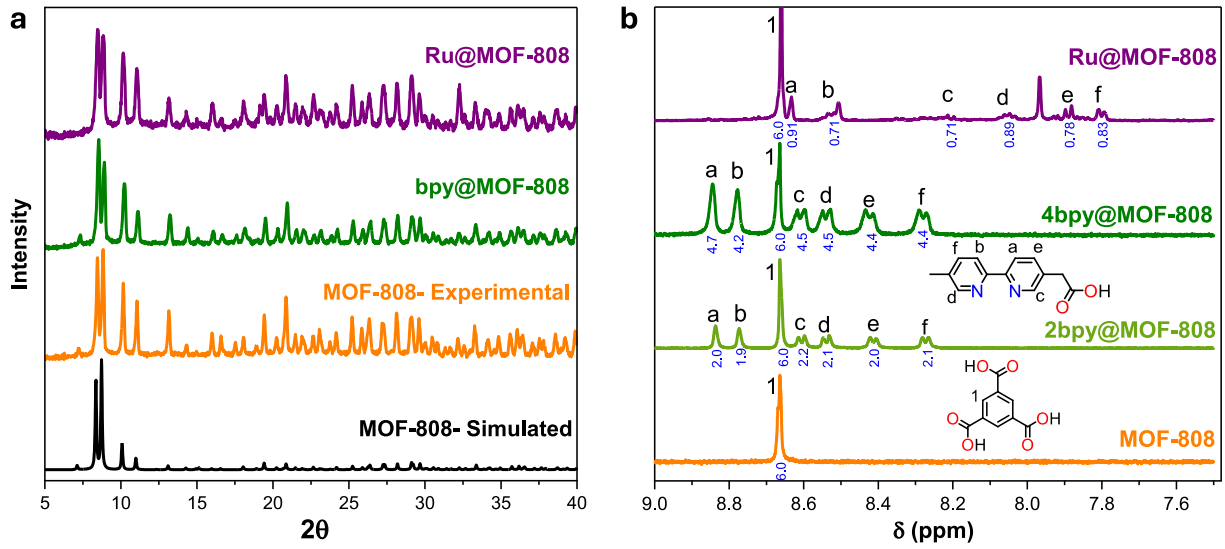

Figure 1. a) pXRD of MOF-808, bpy@MOF-808 (2bpy/node) and Ru@MOF-808. The simulated pXRD was obtained from using the structure obtained using single-crystal XRD.[40] b) ^{1}H NMR spectra of D_2O solutions after the MOF digestion (MOF-808 and bpy@MOF-808 were acid-digested, while Ru@MOF-808 was base-digested).

The spectroscopic characterization of post-synthetically modified MOF-808 was achieved using UV-Vis reflectance and X-ray absorption (XAS) (Figure 2). The solid-state UV/Vis reflectance data of bpy@MOF-808 and Ru@MOF-808 also indicate that the post-synthetic modification was successful (Figure 2a). The UV/Vis diffuse reflectance of MOF-808 exhibits a feature at 270 nm that is associated with the node-centered electronic transitions.[41] This feature is red-shifted in bpy@MOF-808, which is consistent with the

presence of additional π,π^* electronic transitions associated with the bpy unit. The UV/Vis absorption spectrum of bpy-COOH in acetonitrile exhibits a peak in a similar spectral region, confirming the presence of bpy units in bpy@MOF-808. The UV/Vis reflectance of Ru@MOF-808 exhibits an additional peak in the visible region at 462 nm. This feature is associated with the ^{1}MLCT transition from Ru-centered d-orbitals to π^* tpy or bpy-COOH ligand orbitals. The Ru→tpy ^{1}MLCT feature is expected to appear at 450 nm, based on the UV/Vis absorption spectra of $Ru(tpy)(ACN)_3^{2+}$ and $Ru(tpy)(bpy)ACN^{2+}$ in acetonitrile shown in Figure 2a. (Synthetic details on $Ru(tpy)(bpy)ACN^{2+}$ are provided in supporting information, S1). Analogous complexes have been shown computationally to exhibit Ru→tpy ^{1}MLCT transition in this spectral region.[34] The carboxylated bpy-COOH ligand in Ru@MOF-808 is more electron-withdrawing than 5,5'-dimethyl-2,2'-bipyridine present in the $Ru(tpy)(bpy)ACN^{2+}$ model compound. Thus, the lowest-energy transition in Ru@MOF-808 may be associated with the Ru→bpy-COOH rather than Ru→tpy transition. This difference in lowest-energy transitions may explain the observed red-shift of the absorption spectrum of Ru@MOF-808 relative to that of $Ru(tpy)(bpy)ACN^{2+}$. To further confirm that the Ru-complex coordinates to bpy-COOH, we attempted to coordinate the $Ru(tpy)(ACN)_3^{2+}$ precursor to MOF-808 and this sample showed no significant changes in the UV/Vis spectra, showcasing the need for the bpy groups to attach the Ru complex Figure S5.

A comparison of Ru K-edge EXAFS data for $Ru(tpy)(ACN)_3^{2+}$ and Ru@MOF-808 provides evidence for the coordination of the Ru precursor to the bpy units inside MOF-808 (Figure 2b). The first scattering shells of both complexes, which dominate the intensity of the EXAFS spectra up to R = 2 Å, are relatively similar. The signal consists of a dominant peak at a radial distance of 1.5 pm and is consistent with the presence of six coordinating nitrogen atoms in both samples. The main difference between the two EXAFS patterns is at a radial distance of 2.5 pm, where the $Ru(tpy)(ACN)_3^{2+}$ precursor exhibits a much stronger signal. The second shell scattering fit of the experimental data starting from a DFT-calculated structure reveals that the 2.5 pm peak arises due to the multiple scattering pathway (forward scattering) associated with the carbon atoms in linear acetonitrile and polypyridyl ligands (Details in supporting information, Section 2.2).[42,43] The presence or absence of forward scattering is therefore used here as the distinguishing characteristic between the complexes. In $Ru(tpy)(ACN)_3^{2+}$, the presence of three linear acetonitrile groups results in a particularly strong second shell signal. When two acetonitrile groups are displaced in favor of the nonlinear bpy ligand to obtain Ru@MOF-808, we observe a significant decrease in the second shell intensity. The decreased scattering amplitude indicates the removal of two ACN and the subsequent binding of the bpy cyclometallating ligand.

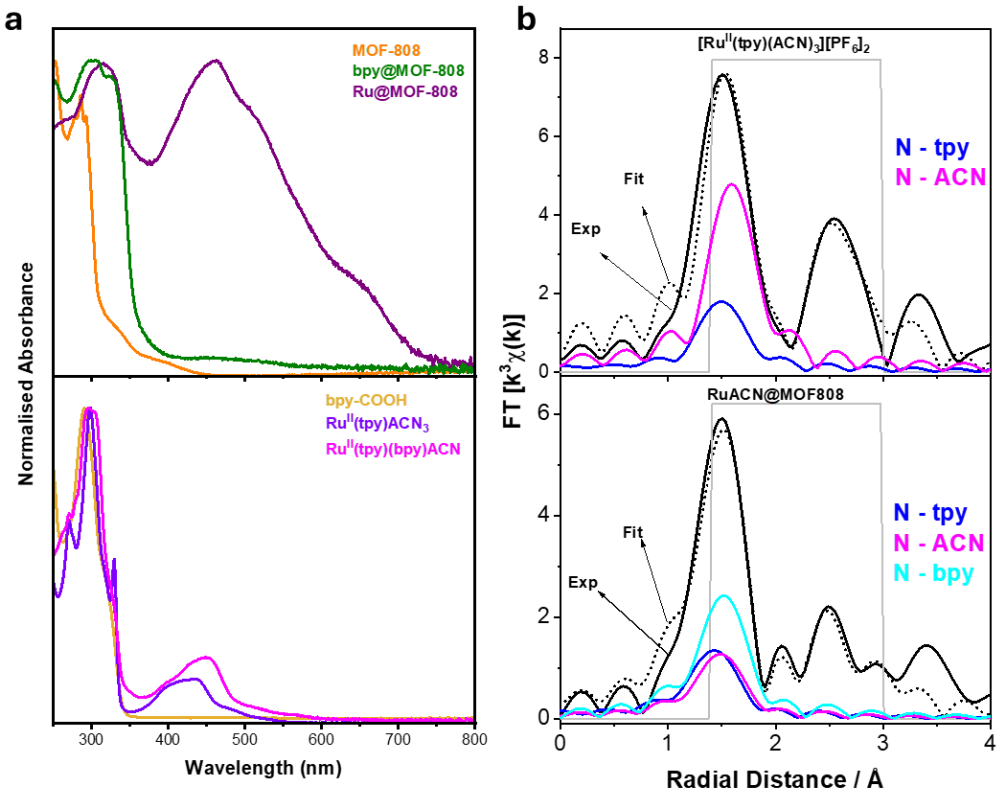

Figure 2. a) Normalized UV-Vis absorption spectra of solid MOF samples (top) and Ru-model compounds in acetonitrile (bottom). b) Ru K-edge EXAFS data and associated fitting of [Ru^{II} (tpy)ACN_3][PF_6] (top) and Ru@MOF-808 (bottom).

The porosity of post-synthetically modified MOFs was evaluated by measuring the nitrogen adsorption isotherms for the four MOF samples (Figure 3a). All MOFs exhibited type I isotherms with a steep increase in adsorbed gas at low partial pressures, consistent with nanometer-sized pores. The experimental data were fitted using the BET model to derive the surface area of each material and the resulting values are plotted in Figure 3b. As expected, the surface area of MOF-808 (1874 m^2/g) is higher than that of bpy@MOF-808 (1228 m^2/g for the sample with 2 bpy/node and 457 m^2/g for 4bpy/node). The surface area of Ru@MOF-808 (1323 m^2/g) was higher than that of the precursor bpy@MOF-808 with 2bpy/node. This result is consistent with the NMR results shown in Figure 1b that illustrate that half of the bpy units are removed from the MOF during the reaction with $Ru(tpy)(ACN)_3^{2+}$. It is interesting that Ru@MOF-808 exhibits an adsorption/desorption hysteresis, and this behavior is likely associated with the presence of very small pores within Ru@MOF-808 where nitrogen accessibility is restricted at 77 K and equilibrium is not achieved within the equilibration time of the experiment.[44]

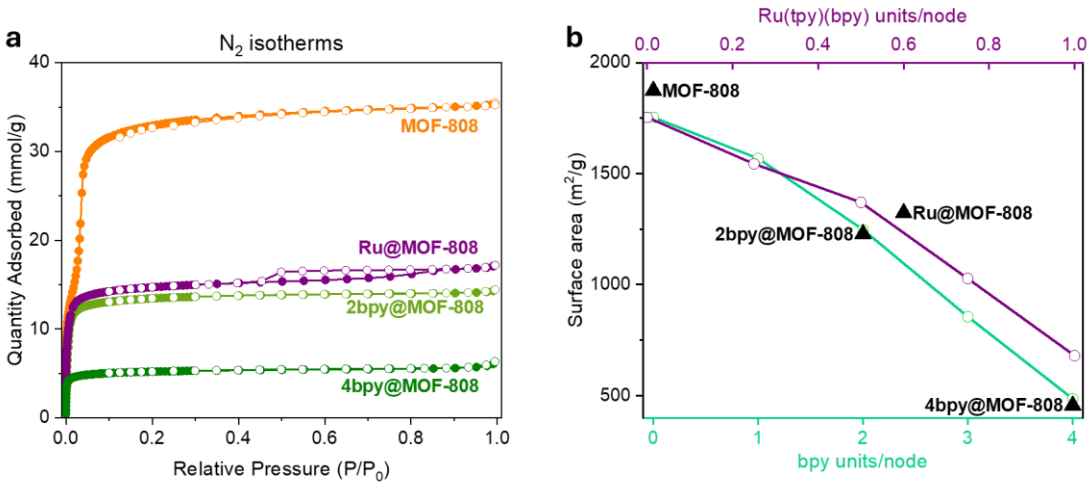

Figure 3. a) N2 adsorption-desorption isotherm at 77K on MOF-808, Ru@MOF-808, 2bpy@MOF-808, and 4bpy@MOF-808. b) Comparison between experimental (▲) and calculated (◯) surface area for MOF-808, 2bpy@MOF-808, 4bpy@MOF-808, and Ru@MOF-808 as a function of bpy unit per node (bottom x-axis) and Ru(tpy)(bpy) unit (top x-axis).

To further understand the changes observed in experimental adsorption isotherms, we performed molecular dynamics simulations for MOF-808 with a varying number of bpy-COOH units per node (computational details described in Section S4 of the supporting information). The optimized structures of bpy@MOF-808 containing either two or four bpy/node demonstrate our intuition that the kinetics of bpy ligand attachment to the surface of the node may be sterically hindered as the synthesis progresses (Figure 4). This implies not all surface sites are converted from activated H_2O/OH to bpy-COOH. In addition, the simulation cell of MOF-808 possesses an open pore volume of ~70%, which goes down to 40% for 2bpy@MOF-808 and 19% for 4bpy@MOF-808. This result is consistent with experimentally obtained values for surface area as shown in Figure 3b. In the case of Ru@MOF-808, a linear drop in the percentage of the open pore volume is calculated with the addition of a Ru(tpy)(bpy) unit terminating at 31% open pore volume for a simulation cell with one unit loading on each node.

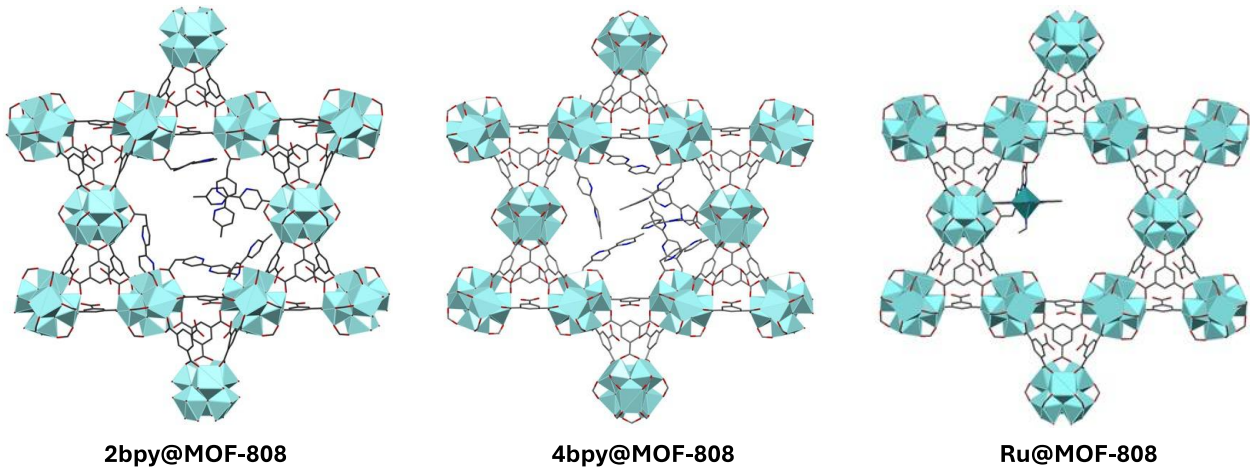

Figure 4. Structures for MOF-808 modified with 2bpy, 4bpy and Ru(tpy)(bpy)ACN^{2+} simulated using Vienna Ab initio Simulation Package (VASP) using Projected Augmented Wave (PAW) formalism.

The optimized structures with different bpy and Ru loadings were then used to calculate the surface area using the Monte Carlo Widom N_2 insertion technique. We find an exceptional agreement between experimental (1874 m^2/g) and calculated (1754 m^2/g) surface areas (see Figure 3b) for MOF-808, while for bpy@MOF-808, the experimental and calculated values for the 2bpy/node loading are 1228 m^2/g and 1247 m^2/g, respectively. We also ran molecular dynamics simulations for Ru@MOF-808 at varying loadings of Ru-complex. We find that the amount of Ru-complex loading is greatly affected by the sterics and that the loadings of more than one Ru cluster per node lead to almost complete loss of accessible surface area (Figure 3b). The calculated surface area as a function of Ru-loading shows that the loading of 0.6 Ru clusters resulted in a surface area value that is in good agreement with the observed experimental value (1233 vs. 1323 m^2/g). Overall, our combined experimental and computational work indicates successful post-synthetic modification of MOF-808 at the loading of 2bpy/node for bpy@MOF-808 and 0.6Ru/node for Ru@MOF-808.

Photochemical CO_2 Reduction by Ru@MOF-808

The photocatalytic CO_2 reduction by Ru@MOF-808 was evaluated under several different experimental conditions (Figure 5a and Supporting Information) and CO and $HCOO^-$ were found to be formed in all these situations. MOF-808, under photochemical conditions, failed to perform CO_2 reduction, pointing to Ru(tpy)(bpy)ACN^{2+} as the source for the observed activity (Figure S7). Among the sacrificial electron donors tested (TEOA, BNAH, BIH), BIH was found to be crucial in initiating the catalytic cycle, likely by reductive quenching the excited state of the Rutpybpy unit ($Ru^{(2+*/1+)}$= 1.01 V vs NHE).[45] This result is consistent with the fact that BIH is the strongest reductant ($E_{1/2}^0$ (BIH/BIH$^{\bullet+}$) = 0.56 V; $E_{1/2}^0$ (BNAH/BNAH$^{\bullet+}$)= 0.89 V; $E_{1/2}^0$ (TEOA/TEOA$^{\bullet+}$)= 1.07 V).[46,47] The addition of TEOA along with BIH resulted in an increase of the formate yield, while little variation was found in CO production as shown in Figure 5a. This finding is consistent with a previous report

by Fujita and co-authors, who showed that TEOA captures carbon dioxide into a zwitterionic alkyl carbonate adduct and has a vital role in the catalytic generation of formate by enhancing the hydride transfer kinetics by several orders of magnitude.[22] However, TEOA has a negative effect on our framework and has led to the gradual disintegration of Ru@MOF-808.

It is interesting that, even in the absence of TEOA, some amount of formate was observed, indicating the possible role of MOF-808 in exhibiting similar CO_2 capture and hydride transfer kinetics enhancements as TEOA. To evaluate this effect, we performed comparative photocatalytic experiments for Ru@MOF-808 and the corresponding model compound in the absence of framework, Rutpybpy-ACN, by ensuring an equal amount of Ru sites in both cases. These experiments were conducted in CO_2-saturated ACN/H_2O solvent mixture in the presence of BIH alone as the electron donor. Interestingly, this study revealed that Rutpybpy-ACN generates more CO, whereas Ru@MOF-808 outperformed the former in formate production, as shown in Figures 5b and 5c. Control experiments were conducted to reveal the role of each component involved in photocatalysis (Supporting Information, Table S3, Entries 8 and 10-12). Neither CO nor formate was detected in the absence of light and Ru@MOF-808 indicating the process is purely photon-mediated and that Ru centers are essential for catalysis. In the absence of water, the formation of reduced products is heavily suppressed, suggesting that water might be acting as a proton relay or proton source. Similar effects of water on catalytic CO_2 reduction have been reported previously.[48,49] The photoirradiated mixture in the absence of CO_2 was incapable of producing CO and formate, justifying the origin of obtained reduced chemicals is from the supplied CO_2. In addition, the structural integrity of Ru@MOF-808 after photocatalysis was found to be preserved with a minimal extent of damage, as indicated by pXRD (Figure S8).

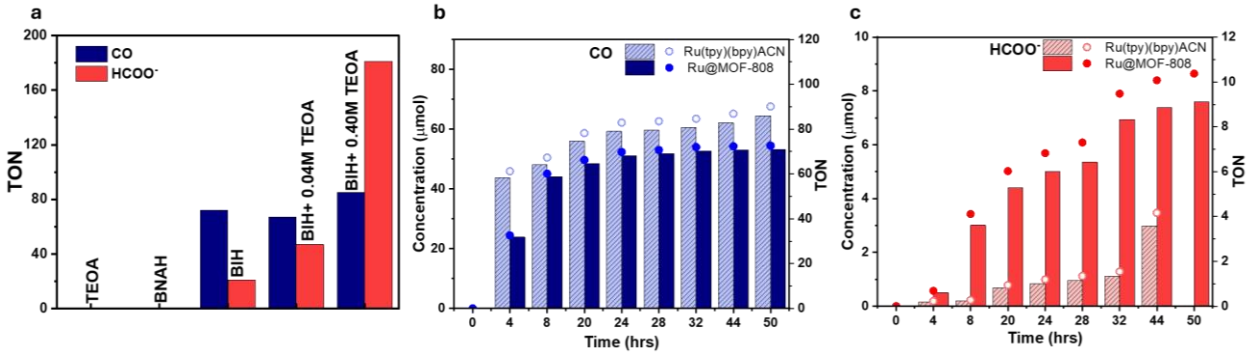

Figure 5. a) Photochemical studies using Ru@MOF-808 under different experimental conditions (Details in supporting information, Table S3, Entries 3-5). Photocatalytic CO_2 reduction studies on Ru@MOF-808 and Ru(tpy)(bpy)ACN^{2+} in the presence of BIH alone showing b) CO and c) $HCOO^-$ generation (bar columns represent concentration in μmol and scatters represent TON, Supporting information, S3.2).

The difference observed in the CO/formate ratios between Ru@MOF-808 and Rutpybpy-ACN suggests that the framework somehow facilitates the formate formation. This finding is particularly interesting in light of our recent findings that the Zr-nodes play an important role in capturing carbon dioxide in the form of Zr-bicarbonate species, which are photochemically reduced to the formate in the presence of appropriate sacrificial donors.[50] The formation of CO likely follows a mechanism involving a Ru-COOH intermediate (Supporting information, scheme S1) as proposed previously for similar catalysts. [27,37] Here, we focus on the increased formate selectivity and hypothesize a cooperative mechanism involving CO_2 capture by Zr-based nodes and a subsequent hydride transfer from photochemically generated Ru-hydride to the neighboring Zr-bicarbonate of the node, as shown in Figure 6. The proposed mechanism starts with the capture of carbon dioxide by the MOF node to form the Zr-bicarbonate intermediate Ru@MOF-808-bicarb1. The proposed photochemical step involves reductive quenching of the photoexcited Rutpybpy unit in Ru@MOF-808 using BIH as the sacrificial donor to form the Ru-hydride intermediate Ru-H@MOF-808-bicarb1. While this process involves an overall transfer of the hydride ion, it likely occurs via a sequence of electron and proton transfer steps, as was previously shown for the molecular analog.[36]

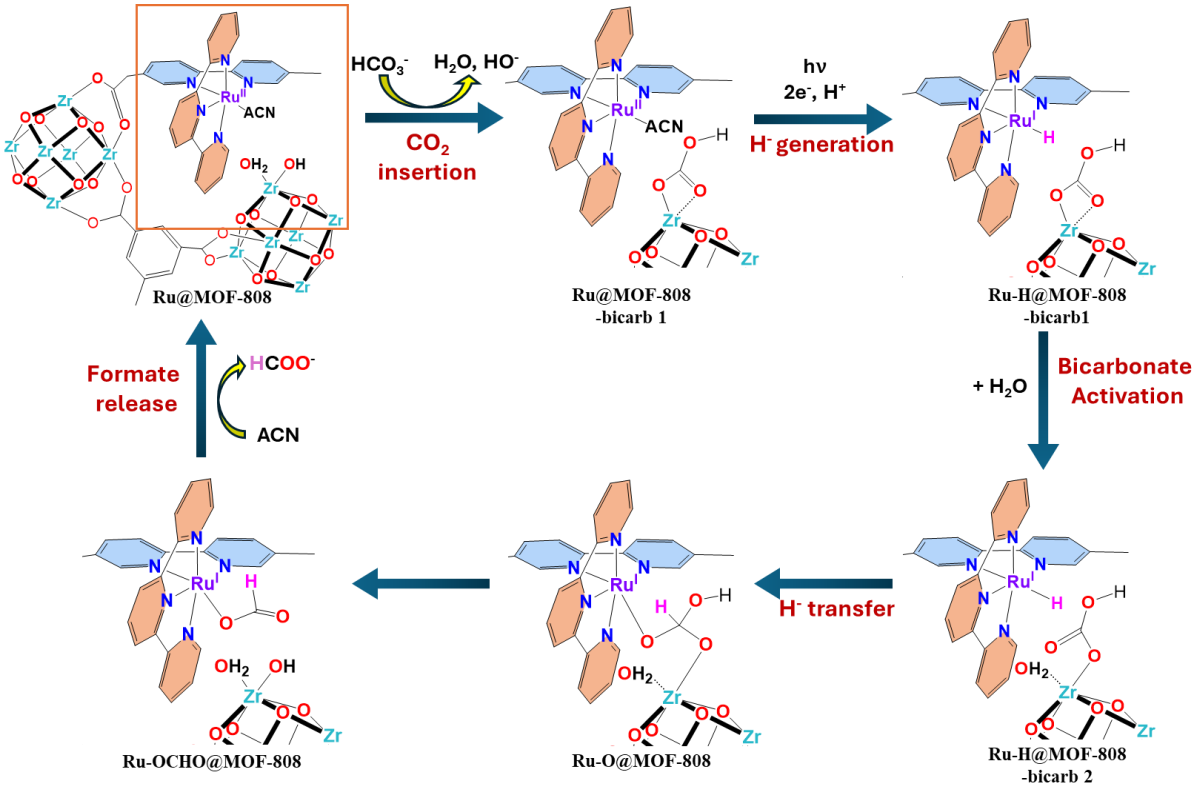

Figure 6. Schematic illustration of the proposed mechanistic pathway towards the formation of $HCOO^-$ by Ru@MOF-808 under photocatalytic conditions. (For clarity, the square boxed part in the top left corner structure is used to depict the possible intermediates).

The bidentate Zr-bicarbonate intermediate Ru-H@MOF-808-bicarb1 is too rigid, preventing the Ru-H and bicarbonate moieties from coming into the close contact needed for the hydride transfer process. We derive this conclusion from our computational search for close contacts between two moieties, which resulted in three plausible structures involving either one or two Zr-nodes, as shown in Figure S9. Even though these structures bring Ru-H within a few Angstroms of the bicarbonate C-atom, their geometry is such that the hydride transfer is not likely to occur. Thus, we hypothesize that the zirconium-bound bicarbonate needs to be further activated by converting into a more flexible monodentate intermediate Ru-H@MOF-808-bicarb2. The subsequent hydride and proton transfer are proposed to generate Ru-bound formate, which is further released to close the catalytic cycle. Computational analysis of this mechanism will be evaluated in the follow-up study.

In summary, we report the photocatalytic CO_2 reduction by Ru@MOF-808, a porous Zr-based MOF that has been post-synthetically modified with a well-known Ru-based catalyst, $Ru(tpy)(bpy)^{2+}$. Our extensive experimental characterization of Ru@MOF-808, supported by theoretical calculations, revealed that the Ru-moieties are incorporated at a loading of almost one Ru per Zr node. The photochemical CO_2 reduction was evaluated in the presence of several sacrificial electron donors and we found that only BIH is sufficiently reducing to enable the reductive quenching of the Ru-based excited state. The CO_2 was reduced to C1 products CO and formate. Interestingly, the formate yield was found to increase in Ru-modified MOF catalyst relative to the performance of the homogeneous Ru-based model analog, indicating that the MOF scaffold increases the formate selectivity. Based on our results and previous literature reports, we propose a mechanism that involves the capture of CO_2 in the form of node-bound Zr-bicarbonate, which is reduced via hydride transfer from the photogenerated Ru-H intermediate. This study demonstrates that the Zr-based MOF nodes provide an ideal platform that not only accommodates photocatalytic units, but also captures CO_2, enabling photoreactive CO_2 capture processes.

Author Contribution

Glusac conceived the project, and Reji designed and performed experiments. Vizuet, Behera, Zheng and Kostopoulos helped in the synthesis and/or characterization of the materials used. Klenk and Zapol performed all periodic DFT calculations and MOF surface area evaluations. Weingartz and Chen helped with the collection and analysis of XAFS data. Yang, Huerta, and Keceli provided computational support by performing DFT calculations on the proposed reaction mechanism.

Acknowledgments

This work is supported by the U.S. Department of Energy (DOE), Office of Science, Office of Basic Energy Science, Division of Chemical Sciences, Geosciences, and Biosciences through Argonne National Laboratory under Contract No. DE-AC02-06CH11357. We thank Mahsa Zarifi for assisting in collecting and summarizing the literature on photophysical and photochemical studies of Ru complexes. Klenk and Zapol gratefully

acknowledge the computing resources provided by the Laboratory Computing Resource Center at Argonne National Laboratory. This research used resources of the Argonne Leadership Computing Facility, a U.S. Department of Energy (DOE) Office of Science user facility at Argonne National Laboratory and is based on research supported by the U.S. DOE Office of Science-Advanced Scientific Computing Research Program, under Contract No. DE-AC02-06CH11357.

TOC Figure:

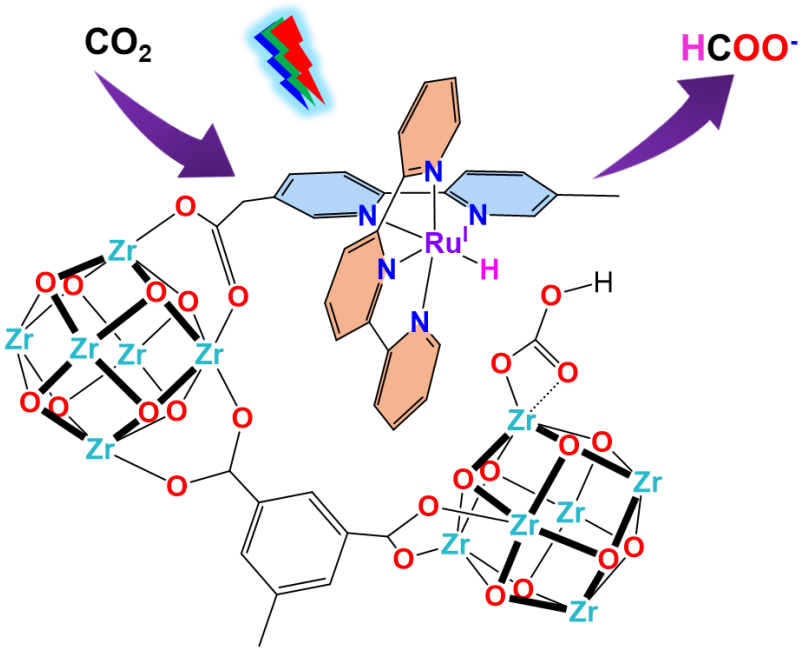

REFERENCE

(1) Aresta, M.; Dibenedetto, A.; Angelini, A. Catalysis for the Valorization of Exhaust Carbon: From CO 2 to Chemicals, Materials, and Fuels. Technological Use of CO 2. *Chem. Rev.* **2014**, *114* (3), 1709–1742. https://doi.org/10.1021/cr4002758.

(2) Yoshino, S.; Iwase, A.; Yamaguchi, Y.; Suzuki, T. M.; Morikawa, T.; Kudo, A. Photocatalytic CO 2 Reduction Using Water as an Electron Donor under Visible Light Irradiation by Z-Scheme and Photoelectrochemical Systems over (CuGa) 0.5 ZnS 2 in the Presence of Basic Additives. *J. Am. Chem. Soc.* **2022**, *144* (5), 2323–2332. https://doi.org/10.1021/jacs.1c12636.

(3) Goeppert, A.; Czaun, M.; Jones, J.-P.; Surya Prakash, G. K.; Olah, G. A. Recycling of Carbon Dioxide to Methanol and Derived Products – Closing the Loop. *Chem. Soc. Rev.* **2014**, *43* (23), 7995–8048. https://doi.org/10.1039/C4CS00122B.

(4) Sun, K.; Qian, Y.; Jiang, H. Metal-Organic Frameworks for Photocatalytic Water Splitting and CO 2 Reduction. *Angew. Chemie Int. Ed.* **2023**, *62* (15). https://doi.org/10.1002/anie.202217565.

(5) Karmakar, S.; Barman, S.; Rahimi, F. A.; Rambabu, D.; Nath, S.; Maji, T. K. Confining Charge-Transfer Complex in a Metal-Organic Framework for Photocatalytic CO2 Reduction in Water. *Nat. Commun.* **2023**, *14* (1), 4508. https://doi.org/10.1038/s41467-023-40117-z.

(6) Li, J.; Huang, H.; Xue, W.; Sun, K.; Song, X.; Wu, C.; Nie, L.; Li, Y.; Liu, C.; Pan, Y.; Jiang, H.-L.; Mei, D.; Zhong, C. Self-Adaptive Dual-Metal-Site Pairs in Metal-Organic Frameworks for Selective CO2 Photoreduction to CH4. *Nat. Catal.* **2021**, *4* (8), 719–729. https://doi.org/10.1038/s41929-021-00665-3.

(7) Karmakar, S.; Barman, S.; Rahimi, F. A.; Maji, T. K. Covalent Grafting of Molecular Photosensitizer and Catalyst on MOF-808: Effect of Pore Confinement toward Visible Light-Driven CO 2 Reduction in Water. *Energy Environ. Sci.* **2021**, *14* (4), 2429–2440. https://doi.org/10.1039/D0EE03643A.

(8) Karmakar, S.; Barman, S.; Rahimi, F. A.; Biswas, S.; Nath, S.; Maji, T. K. Developing Post-Modified Ce-MOF as a Photocatalyst: A Detail Mechanistic Insight into CO 2 Reduction toward Selective C2 Product Formation. *Energy Environ. Sci.* **2023**, *16* (5), 2187–2198. https://doi.org/10.1039/D2EE03755F.

(9) Zhuo, T.-C.; Song, Y.; Zhuang, G.-L.; Chang, L.-P.; Yao, S.; Zhang, W.; Wang, Y.; Wang, P.; Lin, W.; Lu, T.-B.; Zhang, Z.-M. H-Bond-Mediated Selectivity Control of Formate versus CO during CO 2 Photoreduction with Two Cooperative Cu/X Sites. *J. Am. Chem. Soc.* **2021**, *143* (16), 6114–6122. https://doi.org/10.1021/jacs.0c13048.

(10) Feng, X.; Pi, Y.; Song, Y.; Brzezinski, C.; Xu, Z.; Li, Z.; Lin, W. Metal–Organic Frameworks Significantly Enhance Photocatalytic Hydrogen Evolution and CO 2 Reduction with Earth-Abundant Copper Photosensitizers. *J. Am. Chem. Soc.* **2020**, *142* (2), 690–695. https://doi.org/10.1021/jacs.9b12229.

(11) Stanley, P. M.; Thomas, C.; Thyrhaug, E.; Urstoeger, A.; Schuster, M.; Hauer, J.; Rieger, B.; Warnan, J.; Fischer, R. A. Entrapped Molecular Photocatalyst and Photosensitizer in Metal–Organic Framework Nanoreactors for Enhanced Solar CO 2 Reduction. *ACS Catal.* **2021**, *11* (2), 871–882. https://doi.org/10.1021/acscatal.0c04673.

(12) Huang, N.-Y.; He, H.; Liu, S.; Zhu, H.-L.; Li, Y.-J.; Xu, J.; Huang, J.-R.; Wang, X.; Liao, P.-Q.; Chen, X.-M. Electrostatic Attraction-Driven Assembly of a Metal–Organic Framework with a Photosensitizer Boosts Photocatalytic CO 2 Reduction to CO. *J. Am. Chem. Soc.* **2021**, *143* (42), 17424–17430. https://doi.org/10.1021/jacs.1c05839.

(13) Wang, C.; Xie, Z.; DeKrafft, K. E.; Lin, W. Doping Metal–Organic Frameworks for Water Oxidation, Carbon Dioxide Reduction, and Organic Photocatalysis. *J. Am. Chem. Soc.* **2011**, *133* (34), 13445–13454. https://doi.org/10.1021/ja203564w.

(14) Fei, H.; Sampson, M. D.; Lee, Y.; Kubiak, C. P.; Cohen, S. M. Photocatalytic CO 2 Reduction to Formate Using a Mn(I) Molecular Catalyst in a Robust Metal–Organic Framework. *Inorg. Chem.* **2015**, *54* (14), 6821–6828. https://doi.org/10.1021/acs.inorgchem.5b00752.

(15) Stanley, P. M.; Haimerl, J.; Thomas, C.; Urstoeger, A.; Schuster, M.; Shustova, N. B.; Casini, A.; Rieger, B.; Warnan, J.; Fischer, R. A. Host–Guest Interactions in a Metal–Organic Framework Isoreticular Series for Molecular Photocatalytic CO 2 Reduction. *Angew. Chemie Int. Ed.* **2021**, *60* (33), 17854–17860. https://doi.org/10.1002/anie.202102729.

(16) Yang, Y.; Zhang, H.; Wang, Y.; Shao, L.; Fang, L.; Dong, H.; Lu, M.; Dong, L.; Lan, Y.; Zhang, F. Integrating Enrichment, Reduction, and Oxidation Sites in One System for Artificial Photosynthetic Diluted CO 2 Reduction. *Adv. Mater.* **2023**, *35* (40). https://doi.org/10.1002/adma.202304170.

(17) Elgrishi, N.; Chambers, M. B.; Wang, X.; Fontecave, M. Molecular Polypyridine-Based Metal Complexes as Catalysts for the Reduction of CO 2. *Chem. Soc. Rev.* **2017**, *46* (3), 761–796. https://doi.org/10.1039/C5CS00391A.

(18) Chen, Z.; Chen, C.; Weinberg, D. R.; Kang, P.; Concepcion, J. J.; Harrison, D. P.; Brookhart, M. S.; Meyer, T. J. Electrocatalytic Reduction of CO2 to CO by Polypyridyl Ruthenium Complexes. *Chem. Commun.* **2011**, *47* (47), 12607. https://doi.org/10.1039/c1cc15071e.

(19) Assaf, E. A.; Gonell, S.; Chen, C.-H.; Miller, A. J. M. Accessing and Photo-Accelerating Low-Overpotential Pathways for CO 2 Reduction: A Bis-Carbene Ruthenium Terpyridine Catalyst. *ACS Catal.* **2022**, *12* (20), 12596–12606. https://doi.org/10.1021/acscatal.2c03651.

(20) Johnson, B. A.; Agarwala, H.; White, T. A.; Mijangos, E.; Maji, S.; Ott, S. Judicious Ligand Design in Ruthenium Polypyridyl CO 2 Reduction Catalysts to Enhance Reactivity by Steric and Electronic Effects. *Chem. – A Eur. J.* **2016**, *22* (42), 14870–14880. https://doi.org/10.1002/chem.201601612.

(21) Johnson, B. A.; Maji, S.; Agarwala, H.; White, T. A.; Mijangos, E.; Ott, S. Activating a Low Overpotential CO 2 Reduction Mechanism by a Strategic Ligand Modification on a Ruthenium Polypyridyl Catalyst. *Angew. Chemie Int. Ed.* **2016**, *55* (5), 1825–1829. https://doi.org/10.1002/anie.201508490.

(22) Sampaio, R. N.; Grills, D. C.; Polyansky, D. E.; Szalda, D. J.; Fujita, E. Unexpected Roles of Triethanolamine in the Photochemical Reduction of CO2 to Formate by Ruthenium Complexes. *J. Am. Chem. Soc.* **2020**, *142* (5), 2413–2428. https://doi.org/10.1021/jacs.9b11897.

(23) Ishida, H.; Tanaka, H.; Tanaka, K.; Tanaka, T. Selective Formation of HCOO – in the Electrochemical CO 2 Reduction Catalysed by [Ru(Bpy) 2 (CO) 2] 2+ (Bpy = 2,2′-Bipyridine). *J. Chem. Soc., Chem. Commun.* **1987**, No. 2, 131–132. https://doi.org/10.1039/C39870000131.

(24) Ishida, H.; Tanaka, K.; Tanaka, T. Electrochemical CO2 Reduction Catalyzed by

Ruthenium Complexes [Ru(Bpy)2(CO)2]2+ and [Ru(Bpy)2(CO)Cl]+. Effect of PH on the Formation of CO and HCOO-. *Organometallics* **1987**, *6* (1), 181–186. https://doi.org/10.1021/om00144a033.

(25) Agarwala, H.; Chen, X.; Lyonnet, J. R.; Johnson, B. A.; Ahlquist, M.; Ott, S. Alternating Metal-Ligand Coordination Improves Electrocatalytic CO 2 Reduction by a Mononuclear Ru Catalyst**. *Angew. Chemie* **2023**, *135* (17). https://doi.org/10.1002/ange.202218728.

(26) Chen, Z.; Chen, C.; Weinberg, D. R.; Kang, P.; Concepcion, J. J.; Harrison, D. P.; Brookhart, M. S.; Meyer, T. J. Electrocatalytic Reduction of CO2 to CO by Polypyridyl Ruthenium Complexes. *Chem. Commun.* **2011**, *47*, 12607–12609. https://doi.org/http://dx.doi.org/10.1039/C1CC15071E.

(27) Schneider, T. W.; Hren, M. T.; Ertem, M. Z.; Angeles-Boza, A. M. [Ru II (Tpy)(Bpy)Cl] + -Catalyzed Reduction of Carbon Dioxide. Mechanistic Insights by Carbon-13 Kinetic Isotope Effects. *Chem. Commun.* **2018**, *54* (61), 8518–8521. https://doi.org/10.1039/C8CC03009J.

(28) Kern, S.; van Eldik, R. Mechanistic Insight from Activation Parameters for the Reaction of a Ruthenium Hydride Complex with CO 2 in Conventional Solvents and an Ionic Liquid. *Inorg. Chem.* **2012**, *51* (13), 7340–7345. https://doi.org/10.1021/ic300718v.

(29) Pugh, J. R.; Bruce, M. R. M.; Sullivan, B. P.; Meyer, T. J. Formation of a Metal-Hydride Bond and the Insertion of Carbon Dioxide. Key Steps in the Electrocatalytic Reduction of Carbon Dioxide to Formate Anion. *Inorg. Chem.* **1991**, *30* (1), 86–91. https://doi.org/10.1021/ic00001a016.

(30) Matsubara, Y.; Fujita, E.; Doherty, M. D.; Muckerman, J. T.; Creutz, C. Thermodynamic and Kinetic Hydricity of Ruthenium(II) Hydride Complexes. *J. Am. Chem. Soc.* **2012**, *134* (38), 15743–15757. https://doi.org/10.1021/ja302937q.

(31) Konno, H.; Kobayashi, A.; Sakamoto, K.; Fagalde, F.; Katz, N. E.; Saitoh, H.; Ishitani, O. Synthesis and Properties of [Ru(Tpy)(4,4′-X2bpy)H]+ (Tpy=2,2′:6′,2″-Terpyridine, Bpy=2,2′-Bipyridine, X=H and MeO), and Their Reactions with CO2. *Inorganica Chim. Acta* **2000**, *299* (2), 155–163. https://doi.org/10.1016/S0020-1693(99)00488-0.

(32) Nagao, H.; Mizukawa, T.; Tanaka, K. Carbon-Carbon Bond Formation in the Electrochemical Reduction of Carbon Dioxide Catalyzed by a Ruthenium Complex. *Inorg. Chem.* **1994**, *33* (15), 3415–3420. https://doi.org/10.1021/ic00093a033.

(33) Müller, A. V.; Ahmad, S.; Sirlin, J. T.; Ertem, M. Z.; Polyansky, D. E.; Grills, D. C.; Meyer, G. J.; Sampaio, R. N.; Concepcion, J. J. Reduction of CO to Methanol with Recyclable Organic Hydrides. *J. Am. Chem. Soc.* **2024**, *146* (15), 10524–10536. https://doi.org/10.1021/jacs.3c14605.

(34) Jakubikova, E.; Chen, W.; Dattelbaum, D. M.; Rein, F. N.; Rocha, R. C.; Martin,

R. L.; Batista, E. R. Electronic Structure and Spectroscopy of [Ru(Tpy) 2] 2+ , [Ru(Tpy)(Bpy)(H 2 O)] 2+ , and [Ru(Tpy)(Bpy)(Cl)] +. *Inorg. Chem.* **2009**, *48* (22), 10720–10725. https://doi.org/10.1021/ic901477m.

(35) Siewert, B.; Langerman, M.; Hontani, Y.; Kennis, J. T. M.; van Rixel, V. H. S.; Limburg, B.; Siegler, M. A.; Talens Saez, V.; Kieltyka, R. E.; Bonnet, S. Turning on the Red Phosphorescence of a [Ru(Tpy)(Bpy)(Cl)]Cl Complex by Amide Substitution: Self-Aggregation, Toxicity, and Cellular Localization of an Emissive Ruthenium-Based Amphiphile. *Chem. Commun.* **2017**, *53* (81), 11126–11129. https://doi.org/10.1039/C7CC02989F.

(36) Matsubara, Y.; Konno, H.; Kobayashi, A.; Ishitani, O. Quantitative Photochemical Formation of [Ru(Tpy)(Bpy)H] +. *Inorg. Chem.* **2009**, *48* (21), 10138–10145. https://doi.org/10.1021/ic901080r.

(37) Lee, S. K.; Kondo, M.; Okamura, M.; Enomoto, T.; Nakamura, G.; Masaoka, S. Function-Integrated Ru Catalyst for Photochemical CO 2 Reduction. *J. Am. Chem. Soc.* **2018**, *140* (49), 16899–16903. https://doi.org/10.1021/jacs.8b09933.

(38) Queyriaux, N.; Swords, W. B.; Agarwala, H.; Johnson, B. A.; Ott, S.; Hammarström, L. Mechanistic Insights on the Non-Innocent Role of Electron Donors: Reversible Photocapture of CO 2 by Ru II -Polypyridyl Complexes. *Dalt. Trans.* **2019**, *48* (45), 16894–16898. https://doi.org/10.1039/C9DT03461G.

(39) Aunan, E.; Affolter, C. W.; Olsbye, U.; Lillerud, K. P. Modulation of the Thermochemical Stability and Adsorptive Properties of MOF-808 by the Selection of Non-Structural Ligands. *Chem. Mater.* **2021**, *33* (4), 1471–1476. https://doi.org/10.1021/acs.chemmater.0c04823.

(40) Furukawa, H.; Gándara, F.; Zhang, Y.-B.; Jiang, J.; Queen, W. L.; Hudson, M. R.; Yaghi, O. M. Water Adsorption in Porous Metal–Organic Frameworks and Related Materials. *J. Am. Chem. Soc.* **2014**, *136* (11), 4369–4381. https://doi.org/10.1021/ja500330a.

(41) Yi, K.; Li, H.; Zhang, X.; Zhang, L. Designed Tb(III)-Functionalized MOF-808 as Visible Fluorescent Probes for Monitoring Bilirubin and Identifying Fingerprints. *Inorg. Chem.* **2021**, *60* (5), 3172–3180. https://doi.org/10.1021/acs.inorgchem.0c03312.

(42) Liu, J.; Frenkel, A. I. Multiple-Scattering EXAFS Analysis; 2022. https://doi.org/10.1107/S1574870721010922.

(43) Co, M. S.; Hendrickson, W. A.; Hodgson, K. O.; Doniach, S. Multiple-Scattering Effects in EXAFS Spectroscopy of Oxygen-Bridged Iron Complexes. Possibility of Angle Determination of EXAFS Analysis. *J. Am. Chem. Soc.* **1983**, *105* (5), 1144–1150. https://doi.org/10.1021/ja00343a013.

(44) Silvestre-Albero, A. M.; Juárez-Galán, J. M.; Silvestre-Albero, J.; Rodríguez-Reinoso, F. Low-Pressure Hysteresis in Adsorption: An Artifact? *J. Phys. Chem. C* **2012**, *116* (31), 16652–16655. https://doi.org/10.1021/jp305358y.

(45) Bock, C. R.; Connor, J. A.; Gutierrez, A. R.; Meyer, T. J.; Whitten, D. G.; Sullivan, B. P.; Nagle, J. K. Estimation of Excited-State Redox Potentials by Electron-Transfer Quenching. Application of Electron-Transfer Theory to Excited-State Redox Processes. *J. Am. Chem. Soc.* **1979**, *101* (17), 4815–4824. https://doi.org/10.1021/ja00511a007.

(46) Zhu, X.-Q.; Zhang, M.-T.; Yu, A.; Wang, C.-H.; Cheng, J.-P. Hydride, Hydrogen Atom, Proton, and Electron Transfer Driving Forces of Various Five-Membered Heterocyclic Organic Hydrides and Their Reaction Intermediates in Acetonitrile. *J. Am. Chem. Soc.* **2008**, *130* (8), 2501–2516. https://doi.org/10.1021/ja075523m.

(47) Manke, A.-M.; Geisel, K.; Fetzer, A.; Kurz, P. A Water-Soluble Tin(<scp>iv</Scp>) Porphyrin as a Bioinspired Photosensitiser for Light-Driven Proton-Reduction. *Phys. Chem. Chem. Phys.* **2014**, *16* (24), 12029–12042. https://doi.org/10.1039/C3CP55023K.

(48) Lim, C.-H.; Holder, A. M.; Musgrave, C. B. Mechanism of Homogeneous Reduction of CO 2 by Pyridine: Proton Relay in Aqueous Solvent and Aromatic Stabilization. *J. Am. Chem. Soc.* **2013**, *135* (1), 142–154. https://doi.org/10.1021/ja3064809.

(49) Wang, Y.; Liu, T.; Chen, L.; Chao, D. Water-Assisted Highly Efficient Photocatalytic Reduction of CO 2 to CO with Noble Metal-Free Bis(Terpyridine)Iron(II) Complexes and an Organic Photosensitizer. *Inorg. Chem.* **2021**, *60* (8), 5590–5597. https://doi.org/10.1021/acs.inorgchem.0c03503.

(50) Zheng, X.; Drummer, M. C.; He, H.; Rayder, T. M.; Niklas, J.; Weingartz, N. P.; Bolotin, I. L.; Singh, V.; Kramar, B. V.; Chen, L. X.; Hupp, J. T.; Poluektov, O. G.; Farha, O. K.; Zapol, P.; Glusac, K. D. Photoreactive Carbon Dioxide Capture by a Zirconium–Nanographene Metal–Organic Framework. *J. Phys. Chem. Lett.* **2023**, *14* (18), 4334–4341. https://doi.org/10.1021/acs.jpclett.3c00049.